Sustainable Energy & Fuels

ROYAL SOCIETY OF CHEMISTRY

PAPER

View Article Online
View Journal | View Issue

Check for updates

Cite this: *Sustainable Energy Fuels*, 2021, **5**, 5270

Thermal annealing effects on hydrothermally synthesized unsupported MoS_2 for enhanced deoxygenation of propylguaiacol and kraft lignin†

You Wayne Cheah,[a] Muhammad Abdus Salam,[a] Joby Sebastian,[a] Sreetama Ghosh,[a] Olov Öhrman,[b] Derek Creaser [a] and Louise Olsson *[a]

Catalytic hydrodeoxygenation (HDO) is an important hydrotreating process that is used to improve the quality of bio-oils to produce biomass-derived fuel components and chemicals. Molybdenum disulfide (MoS_2) has been widely used as a catalyst in hydrodesulfurization (HDS) applications for several decades, which can be further improved for effective unsupported catalyst synthesis. Herein, we studied a universally applicable post-annealing treatment to a hydrothermally synthesized MoS_2 catalyst towards developing efficient unsupported catalysts for deoxygenation. The effect of the annealing treatment on the catalyst was studied and evaluated for HDO of 4-propylguaiacol (PG) at 300 °C with 50 bar H_2 pressure. The annealing of the as-synthesized catalyst under nitrogen flow at 400 °C for 2 h was found to enhance the HDO activity. This enhancement is largely induced by the changes in the microstructure of MoS_2 after the annealing in terms of slab length, stacking degree, defect-rich sites and the MoS_2 edge-to-corner site ratio. Besides, the effect of hydrothermal synthesis time and acid addition combined with the annealing treatment on the MoS_2 catalytic activity was also studied for the same model reaction. The annealed MoS_2 with a synthesis time of 12 h under an acidic environment was found to have improved crystallinity and exhibit the highest deoxygenation degree among all the studied catalysts. An acidic environment during the synthesis was found to be crucial in facilitating the growth of MoS_2 micelles, resulting in smaller particles that affected the HDO activity. The annealed unsupported MoS_2 with the best performance for PG hydrodeoxygenation was further evaluated for the hydrotreatment of kraft lignin and demonstrated a high deoxygenation ability. The results also indicate a catalyst with high activity for deoxygenation and hydrogenation reactions can suppress char formation and favor a high lignin bio-oil yield. This research uncovers the importance of a facile pretreatment on unsupported MoS_2 for achieving highly active HDO catalysts.

Received 3rd May 2021
Accepted 14th September 2021

DOI: 10.1039/d1se00686j

rsc.li/sustainable-energy

1. Introduction

The continuous increase in global emissions of greenhouse gases (GHG) from the burning of fossil fuels and the depleting fossil fuel reserves have prompted the search for alternative renewable fuels.[1] Lignin, a complex three-dimensional biopolymer that accounts for 15–30% of the dry weight of lignocellulosic biomass is often underutilized and burnt to produce excess utility heat for the paper processing industry.[2] It consists of methoxylated monolignol monomers (*e.g.* coniferyl, sinapyl, and *p*-coumaryl alcohol) that are largely linked together by different C–C and C–O bonds.[3] The breakdown of these linkages is required to obtain low molecular weight compounds for further upgrading. Lignin-derived bio-oil, a potential advanced biofuel obtained from the fast pyrolysis or thermal liquefaction of lignin, can be seen as an attractive option for alternative fuels.[4–6] However, the bio-oil produced using these depolymerization techniques contains a large amount of oxygenates like phenolics, alcohol, and ketone compounds that require an upgrading process for further use. The high oxygen content leads to several undesirable characteristics like low pH value, high viscosity, and low heating value as a transportation fuel.[7] Hence, catalytic hydrodeoxygenation (HDO), a hydrotreating process can be adopted to remove excess oxygen in the form of water using hydrogen as a co-reactant and facilitated by the use of selective hydrotreating catalysts.[8]

The selection of an active and selective HDO catalyst is crucial in accelerating HDO reactions. The widely used sulfided transition metal catalysts (TMS) in the hydroprocessing unit for hydrodesulfurization (HDS) and hydrodenitrogenation (HDN) appear to be transferable and applicable to the HDO

[a]*Competence Centre for Catalysis, Department of Chemical Engineering, Chalmers University of Technology, Gothenburg, 41296, Sweden. E-mail: louise.olsson@chalmers.se*

[b]*Preem AB, Sweden*

† Electronic supplementary information (ESI) available. See DOI: 10.1039/d1se00686j

technology. The sulfur content (1–2 wt%) in kraft lignin due to the pulping process can act as a poison to some catalyst systems like noble metal catalysts.[9] Hence, the use of sulfur tolerant catalysts like TMS can be beneficial and relevant when applied to the hydrotreatment of kraft lignin.

The traditional TMS catalysts are the typical molybdenum sulfide catalyst supported on γ-alumina promoted by nickel (Ni) or cobalt (Co).[10] Over the past few decades, the development of these supported Ni(Co)MoS hydrotreating catalysts has reached a mature stage with the possibility to enhance its performance by either replacing the alumina carrier with others such as carbon[11–15] or omitting the use of a support.[16] A good example of an unsupported catalyst system is the NEBULA technology that has been jointly established by ExxonMobil and Albemarle Catalysts.[16,17] This commercialized and patented technology has been able to show the superior activity of the unsupported catalysts as compared to the conventional hydroprocessing catalysts.[17] Another application of the unsupported hydroprocessing catalysts was the Eni Slurry Technology (EST) process.[18] The EST process uses highly dispersed MoS_2 nanoparticles formed by the oleo-soluble molybdenum precursor co-feeded with heavy oil feedstocks under reaction conditions of 400–450 °C and 150 bar with a continuous hydrogen flow resulting in high hydrogenation activity.[18] Furthermore, the promising results were demonstrated in a recent study using unsupported Mo precursors for the co-processing of fast pyrolysis bio-oil (FPBO) with heavy fossil feedstocks in a slurry hydrocracking unit.[19] Besides, it is worth mentioning that kraft lignin has a high molecular weight of typically around 16.7 kDa.[20] The diffusion of huge lignin polymeric molecules through porous support materials to access the active sites of a supported catalyst poses a significant obstacle to the process. Besides, lignin reactive fragments formed by noncatalytic thermal reactions are thought to repolymerize and form char.[21,22] The transport limitations caused by supported catalysts can hinder the stabilization of these intermediates by hydrogenation reactions and result in greater char formation. Therefore, the use of an unsupported catalyst with high activity seems promising for kraft lignin hydrotreatment.

There are several ways to synthesize molybdenum-based sulfide unsupported catalysts that can be employed in HDO and hydrotreatment processes. For example, Varakin *et al.* prepared unsupported MoS_2 by the support leaching of MoS_2 supported on alumina or carbon-coated alumina which gave a high yield of C18 hydrocarbon in oleic acid HDO.[23] Yoosuk *et al.* synthesized amorphous unsupported MoS_2 and CoMoS catalysts hydrothermally using ammonium tetrathiomolybdate (ATTM) as the catalyst precursor under high hydrogen pressure (28 bar) and high reaction temperature (350 °C).[24] They concluded that the amorphous MoS_2 was selective in cleaving the hydroxyl group in phenol *via* a direct-deoxygenation (DDO) route.[24] Besides, Grilc *et al.* reported the preparation of urchin-like MoS_2 and inorganic-fullerene MoS_2 interconnected by carbon materials *via* the sulphidisation of precursors like MoI_3 and cyclopentadiene–$MoCl_4$, respectively.[25] The results from their work demonstrated that both of these unsupported catalysts gave a high selectivity towards deoxygenation, and possessed a three times higher rate in dehydroxylation as compare to bulk MoS_2.[25] Recently, Zhang *et al.* reported the preparation of few-layer and defect rich MoS_2 and also Co-promoted MoS_2 nanosheets by a one-pot hydrothermal method.[26] These reduced stacking layers and defect-rich MoS_2 could accommodate Co atoms as a promoter and resulted in an active Co–Mo–S phase for *p*-cresol HDO under a low operation reaction temperature of 230 °C.[26]

Among all preparation methods, hydrothermal synthesis seems to be attractive from an industrial point of view for the preparation of unsupported MoS_2, owing to the use of moderate temperature (150–250 °C) and the absence of hydrogen pressure while using ammonium molybdate as the Mo precursor.[27–32] A summary of the deoxygenation application of hydrothermally synthesized unsupported metal sulfides and the main highlight of these studies is provided in Table 1. In all of these studies, the synthesized catalysts were used in the HDO reaction without any pretreatment that can enhance the HDO activity. Herein, we have explored a hydrothermal synthesis method for unsupported MoS_2 catalysts inspired by several preparation methods reported elsewhere.[27–29] We then also further propose an additional annealing process to be applied to the as-synthesized unsupported MoS_2 that changes its structure and morphology that influences its HDO activity. To the best of our knowledge, this is the first work where the main effort has been emphasized on the pretreatment of a hydrothermally synthesized unsupported MoS_2 for deoxygenation enhancement. Synthesis parameters such as the effect of synthesis time and pH adjustment during the synthesis on the morphology of MoS_2 and relative HDO activity were also studied. The activity, selectivity, and effectiveness of the catalysts were first evaluated using an oxygenate model compound, 4-propylguaiacol (PG) that can be obtained from depolymerized lignin fragments. The use of PG in the model reaction has also been shown in our previous work that it is useful to demonstrate the effectiveness of the catalysts for complex lignin hydrotreatment.[33] Hence the catalytic hydrotreatment of kraft lignin was studied using the unsupported MoS_2 showing the best performance for HDO of PG. The comparison between the commercially available bulk MoS_2 and MoS_2 synthesized in this work was made for the HDO of PG and kraft lignin. Besides, the synthesized and annealed unsupported MoS_2 catalysts were characterized in detail by N_2 physisorption, X-ray diffraction (XRD), X-ray photoelectron spectroscopy (XPS), Raman spectroscopy, high-resolution transmission electron microscope (HRTEM), and scanning electron microscopy (SEM) to discover relations between resulting properties of the materials and their catalytic performance. Our research is foreseen to contribute towards a better understanding of the role of a post-thermal annealing treatment on the unsupported MoS_2 for developing highly robust HDO catalysts.

2. Experimental

2.1 Catalyst synthesis

The unsupported MoS_2 catalysts were prepared starting from a simple hydrothermal method following various works from

Wang *et al.*[27,29] incorporating certain modifications in the synthesis steps. 0.35 g of ammonium heptamolybdate tetrahydrate (>99%) and 1.3 g of thiourea (>99%) were both dissolved in 55 ml of distilled water with gentle stirring. The pH of the solution was adjusted to 0.8 using hydrochloric acid (35 wt%). For one catalyst sample, this pH adjustment step was omitted to

Table 1 Overview of literature survey related to the use of hydrothermal synthesized unsupported metal sulfides in deoxygenation application

Unsupported catalysts	Application	Highlights	Ref.
CoMo sulfide and MoS_2	*p*-Cresol hydrodeoxygenation	-Reduced stacking of MoS_2 layers and increased defect sites on basal planes formed more coordinatively unsaturated sites (CUS) to accommodate promoter atoms	26
Co-doped nano sized MoS_2	*p*-Cresol hydrodeoxygenation	-Highly dispersed MoS_2 with abundance of defects and curvy slabs are important features to produce high density of CUS sites and for anchoring Co atoms -Molar ratio of 0.3 for Co/(Co + Mo) gives almost complete *p*-cresol conversion and 98.9% toluene selectivity	30
Ni–Mo sulfides	Palm oil hydrotreating	-Molar ratio of 0.2 for Ni/(Ni + Mo) shows good HDO performance and good recyclability -The incorporation of Ni promoter increased the stacking and layers numbers which also contributed to the increase in the rim and edge sites that is the active site for the hydrogenation reaction	48
Unsupported and supported CoMoS	Waste cooking oil (WCO) hydrotreating	-Unsupported metal sulfides give a higher degree of polymerization due to the lack of acidic sites (absence of catalyst support) -Increased reaction temperature improved deoxygenation, and enhanced the cracking and polymerization degree for unsupported catalyst	31
NiMo and CoMo sulfides	Oleic acid and palmitic hydrodeoxygenation	-Ni promoter decreased the Ni–Mo–S bond strength leading to the formation of CUS on the edges of the MoS_2 slabs -Hydrothermal synthesis of MoS_2 resulted in the bent and folded multi-layered structure of the catalyst	49
CoMoS	*p*-Cresol hydrodeoxygenation	-Optimal hydrothermal temperature is 200 °C -The concentration of Co promoters affects the catalysts surface area, stacking numbers, and also MoS_2 slab length -Increased Co amount hindered and inhibited the MoS_2 growth and caused aggregation of CoS_2 which reduced MoS_2 dispersion yielding longer slabs	27
Ni–Mo–W sulfides	*p*-Cresol hydrodeoxygenation	-Molar ratio of 0.5 for W/Mo gives the highest HDO performance -Optimum molar ratio for W/Mo resulted in the shortest average	32

Table 1 (*Contd.*)

Unsupported catalysts	Application	Highlights	Ref.
		MoS_2 slab length and improved dispersion	
MoS_2 and $CoMoS_2$	Phenol hydrodeoxygenation	-Amorphous and highly bent MoS_2 with multi-layered structure was more active than the crystalline sample -Addition of Co changes the textural properties of the catalysts giving reduced specific surface area and shifted the pore-size distribution to smaller pore sizes	24
NiMo sulfides	Phenol hydrodeoxygenation	-HDO activity depends largely on the sulfide's morphology but not the catalysts surface area -Low layer number in the MoS_2 stack and/or shorter slabs could give higher hydrogenation-dehydration (HYD) activity	50

evaluate its effect on the catalyst properties. The mixed solution was divided equally and transferred to a 70 ml Teflon liner. The filled Teflon liner was placed and sealed in a stainless-steel autoclave. The mixed solution was heated at 200 °C for either 12 h or 24 h. The synthesized catalyst was then filtered and washed with absolute ethanol several times. The filtered and washed catalyst was dried under vacuum at 50 °C overnight. These as-synthesized catalysts were tested without any pretreatment in the model reaction. The as-synthesized catalysts with synthesis times of 12 h and 24 h will be referred to as MoS_2-12 and MoS_2-24, respectively. The dried as-synthesized catalysts were further annealed at 400 °C for 2 h under nitrogen flow before their evaluation in the model reaction. These annealed catalysts with 12 h and 24 h synthesis time will be denoted as MoS_2-12a and MoS_2-24a. Bulk MoS_2 (Sigma-Aldrich) in powdered form with a particle size of ~6 μm (max. 40 μm) was used in the current work for comparison with our in-house synthesized MoS_2. Alumina-supported MoS_2 (13.2 wt% Mo loading) catalyst was also prepared according to the procedure reported by our group earlier[34] for comparison in this work.

2.2 Characterization of unsupported MoS_2

The specific surface area of the catalyst was measured by N_2 physisorption at −196 °C using a TriStar 3000 gas adsorption–desorption analyzer. The catalysts were degassed at 300 °C under nitrogen flow overnight before every measurement for drying purposes. The Brunauer–Emmett–Teller (BET) method was used to calculate the surface areas and the pore sizes were estimated by the Barrett–Joyner–Halenda (BJH) method. XRD measurement was performed using an X-ray powder diffractometer operated at 40 kV and 40 mA (Bruker AXSD8 Advance) with a CuKα monochromatic radiation ($\lambda = 1.542$ Å) source in the 2θ range of 10–80°. XPS measurements were carried out using a PerkinElmer PHI 5000 VersaProbe III Scanning XPS Microprobe. The monochromatic Al-Kα X-ray source with a binding energy of 1486.6 eV was operated in the analysis chamber. The core-level spectra of Mo 3d, O 1s, S 2p, and C 1s were recorded with a step size of 0.1 eV. The raw data was then analyzed using a Shirley background using the software Casa XPS with the C 1s binding energy at 284.8 eV as a reference. The Raman spectra were recorded using a WITec alpha300 R confocal Raman microscope equipped with a thermoelectrically cooled (−60 °C) EMCCD detector. A 532 nm CW diod laser at 0.3 mW was used for excitation and the light was focused on the sample using a 100X/NA0.9 objective. The Raman scattering was collected using the same objective and was spectrally resolved using an 1800 groves per nm grating. Calibration was performed on the position of the Raman spectra bands using the silicon peak at 519.3 nm. The morphologies and structure of the catalysts were obtained by HRTEM on an FEI Titan 80-300 TEM operated at 300 kV equipped with a high angle annular dark-field (HAADF) detector. SEM was performed on a JEOL 7800F Prime to acquire the morphology of the catalysts. The particle diameter of over two hundred MoS_2 particles from the SEM images was measured by ImageJ software and used to obtain average particle sizes.

Quantitative and statistical analyses were performed based on 15–20 representative TEM images taken from different regions of each catalyst. Approximately 500–550 MoS_2 slabs were measured and processed by ImageJ software to calculate the average MoS_2 slab length (ΔL) and stacking number (Δn) using the following equations:[33]

$$\text{Average } MoS_2 \text{ slab length } (\Delta L) = \frac{\sum_i^n x_i l_i}{\sum_i^n x_i} \quad (1)$$

$$\text{Average stacking number } (\Delta n) = \frac{\sum_i^n x_i N_i}{\sum_i^n x_i} \quad (2)$$

i: total number of MoS_2 slabs, N_i: stacking number, l_i: MoS_2 slab length, x_i: number of MoS_2 slabs with N_i layers of length l_i.

Moreover, the MoS_2 dispersion (f_{mo}) was calculated with the following equation reported in the literature:[35]

$$MoS_2 \text{ dispersion } (f_{mo}) = \frac{Mo_{edge}}{Mo_{total}} = \frac{\sum_i^m 6(n_i - 1)}{\sum_i^m (3n_i^2 - 3n_i + 1)} \quad (3)$$

Mo_{edge}: number of Mo atoms that are located on the edges of the MoS_2 slabs, Mo_{total}: total number of Mo atoms, n_i: number of Mo atoms along the edge of MoS_2 slabs with its length obtained by ($L = 3.2(2n_i - 1)$ Å), m: total number of MoS_2 slabs obtained from the TEM images of different catalysts.

The edge-to-corner ratio of MoS_2 slabs was calculated based on the following equation:[36]

$$\frac{f_{edge}}{f_{corner}} = \frac{5\Delta L}{3.2} - 1.5 \quad (4)$$

2.3 Catalytic test for HDO of 4-propylguaiacol (PG)

The catalytic activity was measured using a 300 ml Parr batch reactor. In a typical catalytic test, 66 mg of as-synthesized or annealed unsupported catalyst, 1 g of 4-propylguaiacol, 100 ml of dodecane as the solvent, and 0.5 ml of dimethyl disulfide (DMDS) were loaded into the reactor. The reactor was sealed and first purged three times with N_2 and then followed by H_2. The reactor system was then pressurized to 20 bar of H_2 at room temperature and checked for any leaks. After the leak check, the system was depressurized to 0.1 bar gauge and further heated to a final temperature of 300 °C. It took 25 minutes to reach desired temperature. When the reaction temperature has reached, additional hydrogen was introduced and this point was regarded as the start of the reaction. Reaction conditions for all PG HDO experiments were kept constant at 50 bar H_2, 300 °C, and 1000 rpm for 5 h. All reaction conditions were strictly kept constant during the evaluation of catalytic activities to ensure comparable kinetic results. Reaction liquid product samples were collected every hour during 5 h for further analysis. The withdrawal of the reaction sample caused a drop of *ca.* 1 bar in the reactor which was compensated by repressurizing to 50 bar with hydrogen. The reaction was stopped after 5 h by cooling the reactor with water cooling, followed by releasing the reactor pressure. After pressure release, the reactor was purged with N_2 before opening. The remaining reaction medium was centrifuged to collect all used catalysts. The used catalyst was washed with absolute ethanol several times and dried in an oven at 80 °C overnight.

The PG conversion (C_{PG}), product yield ($Y_{product}$), and selectivity ($S_{product}$) at varying times were calculated based on the following expressions:

$$C_{PG}(\%) = \frac{C_0 - C_t}{C_0} \times 100 \quad (5)$$

$$Y_{product}(\%) = \frac{C_{product,\ t}}{C_0} \times 100 \quad (6)$$

$$S_{product}(\%) = \frac{C_{product,\ t}}{C_0 - C_t} \times 100 \quad (7)$$

C_0: initial PG concentration loaded in the reactor, C_t: PG concentration at a given reaction time, $C_{product,t}$: Product concentration at reaction time.

The units for the yields of reactants and products are expressed as molar percent (mol %). The molar balance for the reaction was assessed by calculating the material balance in the liquid phase. The molar balance was calculated by dividing the summation of the concentration of all identified products by the concentration of the initial PG concentration loaded in the reactor. The calculation is based on the observation that all products detected in the reaction samples retained the six-carbon ring structure of PG. The carbon balance for the liquid phase analysis was found to be ranged over 95–99% for all experiments.

2.4 Hydrotreatment of kraft lignin

The hydrotreatment reaction was carried out in the 300 ml Parr reactor system, the same as that used for the model reaction. Before starting the reaction, the reaction vessel was loaded with 0.75 g of catalysts, 2.25 g of kraft lignin (Sigma Aldrich), and 75 ml of hexadecane as a solvent. The composition of kraft lignin was analyzed by ICP and elemental analysis results are presented in Fig. S1 and Table S1.† The reactor was then sealed and purged with nitrogen three times to remove oxygen traces. The reactor was then pressurized to 40 bar H_2 at room temperature and monitored for leaks during 20 minutes. After a passed leak test, the reaction temperature was set to 340 °C and it took 40 minutes to reach the desired temperature. The stirring rate was set at 1000 rpm when the heating was started. Reaction time zero was recorded once the reaction temperature reached the desired temperature and the reaction was monitored for 5 h with continuous stirring of 1000 rpm. The reactor pressure immediately after reaching 340 °C was 73–76 bar depending on the type of catalyst used in the experiment. The pressure decreased by 1–3 bar to 70–73 bar during the course of the reaction (5 h). After the reaction was completed, all reaction products in liquid form and solid residues in the reaction vessel were collected in a glass bottle for product analysis. The solid residues retained in the reaction medium after the hydrotreatment were obtained by filtering the bio-liquid. The solid residues were washed first with acetone and then dried in an oven at 80 °C overnight. The unconverted lignin retained in the dried solid was dissolved by dimethyl sulfoxide (DMSO) washing. After dissolving the unconverted lignin with DMSO, the solid product was dried again in an oven at 80 °C overnight.

The initial solid residues obtained after filtration should contain spent catalyst, solid char, and unconverted lignin. The weight of the solid was recorded after each drying.

Kraft lignin conversion ($C_{\text{kraft lignin}}$) was calculated based on the following equation:

$$C_{\text{kraft lignin}}(\%) = \frac{\text{initial kraft lignin feed (g)} - \text{unconverted lignin (g)}}{\text{initial kraft lignin feed (g)}} \times 100$$

The amount and yield of solid char were calculated by the following equations:

$$\text{Char amount (g)} = \text{total solid residues (g)} - 0.75\ \text{g of catalyst} - \text{unconverted lignin (g)}$$

$$\text{Char yield (\%)} = \text{char amount (g)}/2.25\ \text{g of initial kraft lignin feed} \times 100\%$$

Individual product selectivity in the bio-liquid were calculated by dividing the corresponding FID peak area of the product by the total FID peak area for all identifiable products in the bio-liquids.

2.5 Product analysis for model compound and kraft lignin hydrotreatment

The reaction products collected during the catalytic reaction for HDO of PG were analyzed by GC-MS (Agilent 7890-5977A, Agilent). The GC was equipped with an HP-5 column (30 m × 250 μm × 0.25 μm), and the injector temperature was kept at 325 °C. The initial oven temperature was 100 °C for 1 minute and then heated to 190 °C at a rate of 10 °C min^{-1}. The heating continued to 300 °C with a ramp of 30 °C min^{-1} and the final temperature was maintained for 80 s.

The bio-liquid products collected after the catalytic hydrotreatment of kraft lignin were analyzed by GC-MS (Agilent 7890-5977A, Agilent). The GC was equipped with an HP-5 column (30 m × 250 μm × 0.25 μm), and the injector temperature was kept at 325 °C. The initial oven temperature was 50 °C for 5 minutes and then heated to 300 °C at a rate of 10 °C min^{-1}. After which the final temperature was maintained constant for 5 minutes.

The bio-liquid products were also analyzed by two-dimensional GC × GC-MS-FID on an Agilent 7890B gas chromatograph equipped with an oven, a flow splitter, a modulator, and a flame ionization detector. The injector temperature was 280 °C and the sample injection volume was 1 μL. Helium gas was used as a carrier gas with a flow rate of 1 ml min^{-1} with a split ratio of 30. The chromatographic separation involves two columns: a mid-polar phase column VF-1701 MS (30 m × 250 μm × 0.25 μm) and a non-polar phase column DB-5MS UI (1.2 m × 150 μm × 0.15 μm). Modulation time on the modulator is 8 s. The oven temperature was initially set at 40 °C for 1 min and then heated up to 280 °C at a rate of 2 °C min^{-1}. The flame ionization detector temperature was set at 250 °C. The analysis was performed using the GCImage software for multidimensional chromatography.

3. Results and discussion

3.1 Catalyst characterization

Table 2 lists the specific surface area, pore-volume, and pore size of the unsupported MoS_2 catalysts in this study, and a bulk MoS_2 sample. The specific surface area decreased in the order: MoS_2-24a > MoS_2-12a > MoS_2-24 > MoS_2-12 > bulk MoS_2. The results suggested that prolonging the synthesis time has a negligible effect on the specific surface area of the synthesized catalyst with MoS_2-24 being 16.2 $m^2\ g^{-1}$ while MoS_2-12 was 15.4 $m^2\ g^{-1}$. However, the specific surface area of the annealed samples of MoS_2-12a and MoS_2-24a were 27.8 $m^2\ g^{-1}$ and 37.1 $m^2\ g^{-1}$, respectively. The N_2 adsorption–desorption isotherms for all studied catalysts are shown in Fig. S2.† The isotherms for the annealed MoS_2 catalysts can be characterized as type IV isotherms following the IUPAC classification.[37] A prominent H3 type hysteresis loop can also be observed for both annealed MoS_2 samples, featuring slit-shaped pores created by the build-up of MoS_2 layers. While for the as-synthesized and bulk MoS_2, type II isotherms can be identified that are distinctive of material with a non-porous character. The observation can be explained by the agglomeration of particles forming larger lumped particles with reduced porosity as will be evident from the SEM images (discussed later in this section). The larger pore size exhibited by the MoS_2-24 also indicates that prolonging the synthesis time resulted in a mixture of large and small particles forming larger cavities. While the results also showed that the annealing process significantly increased the specific surface area and porosity of the unsupported catalysts. It is important to highlight that this porosity was created by the shrinkage of particles during annealing and during the formation of MoS_2 crystals (evident from XRD analysis, discussed later in this section), they were re-coordinated and agglomerated to generate cavities. It is also worth noting that MoS_2-12a has the highest pore volume and the smallest pore size among all unsupported catalysts.

The X-ray diffraction (XRD) patterns for all MoS_2 unsupported catalysts are shown in (Fig. 1a) indicating the crystallinity and phase purity of the MoS_2 catalysts. As can be observed from the XRD patterns, the as-synthesized samples showed a very low crystallinity with a small peak at $2\theta = 14°$ indicating the typical (0 0 2) plane of hexagonal MoS_2. The results confirmed that doubling the synthesis time from 12 h to 24 h did not improve the crystallinity of the samples. On the other hand, for both the annealed MoS_2 samples, prominent peaks can be observed at $2\theta = 14°$, 33°, 39°, and 59° attributed to the (002), (100), (103) and (110) planes of MoS_2.[38] The increase in the crystallinity of the as-synthesized MoS_2 after a simple annealing treatment suggests that the annealing process at 400 °C for 2 h can promote the growth of MoS_2 crystals. In comparison, the bulk MoS_2 is highly crystalline as can be observed from the XRD pattern.

Additionally, Raman spectroscopy was performed to corroborate with XRD patterns and at the same time, to study the chemical state of the as-synthesized and annealed catalysts. The Raman spectrum of MoS_2-24 and MoS_2-24a were obtained

Table 2 Physical properties (surface area, pore-volume, and pore size) and HRTEM analysis of the synthesized unsupported catalysts and bulk MoS_2

Catalysts	Surface area ($m^2\ g^{-1}$)	Pore volume ($cm^3\ g^{-1}$)	Pore size (Å)	Average MoS_2 slab length (ΔL)	Average stacking number (Δn)	MoS_2 dispersion (f_{mo})	Edge-to-corner ratio of MoS_2 slabs
MoS_2-12	15.4	0.34	108	5.07	4.01	0.150	6.42
MoS_2-12a	27.8	0.60	83.8	8.41	2.72	0.103	11.6
MoS_2-24	16.2	0.13	317	6.58	3.26	0.130	8.78
MoS_2-24a	37.1	0.11	105	8.71	3.85	0.105	12.1
Bulk MoS_2	4.70	0.03	177	—	—	—	—

and the results are presented in (Fig. 1b). For MoS_2-24a catalysts, four main Raman peaks located at 379 cm^{-1} (E^1_{2g}), 404 cm^{-1} (A_{1g}), 283 cm^{-1} (E_{1g}), and 454 cm^{-1} (E_{1g}) indicate that the usual 2H–MoS_2 phase can be observed.[39] Moreover, two low-intensity Raman peaks at 219 cm^{-1} and 335 cm^{-1} can be identified in the spectra for MoS_2-24a proving the existence of the 1T phase of MoS_2.[39] The results indicate that the annealing pre-treatment changes the structure of the as-synthesized catalysts and resulted in mixed 1T and 2H phases of MoS_2. In contrast, for MoS_2-24 catalysts, three peaks can be identified as shown in (Fig. 1b) with a relatively lower intensity showing the lower crystallinity of the as-synthesized catalyst.

X-ray photoelectron spectroscopy (XPS) was carried out to determine the chemical state and composition of the unsupported MoS_2 catalysts before and after the annealing treatment (Fig. 2). The Mo 3d spectrum in (Fig. 2a and c) were deconvoluted into three Mo $3d_{5/2}$–Mo $3d_{3/2}$ doublets for the as-synthesized samples. Two characteristic peaks at 229.3 eV and 232.5 eV binding energies correspond to the presence of the Mo^{4+} oxidation state, indicating the MoS_2 species.[40] For the Mo^{5+} oxidation state, characteristic peaks at binding energies 230.0 eV and 233.0 eV can be identified, which demonstrate the presence of intermediate oxysulfide species (MoO_xS_y) in the as-synthesized catalysts.[41] An additional doublet at 233.4 eV and 235.8 eV associated with the Mo^{6+} oxidation state which is associated with the MoO_3 species can be found.[42] Table 3 reports the Mo 3d composition of the Mo states obtained from the XPS data. It can be noticed that the sulfidation degree based on the Mo^{4+} content increased for both annealed MoS_2 as compared to the as-synthesized unsupported catalysts with MoS_2-24a having the highest degree and corresponding lowest degree of oxidation of Mo. The presence of oxysulfide species in the as-synthesized catalysts can be explained by one of the reactions that are expected to occur during the synthesis of MoS_2, where the $(NH_4)_6Mo_7O_{24}$ reacts with H_2S forming MoO_xS_y, ammonia, and water. However, the oxysulfide species

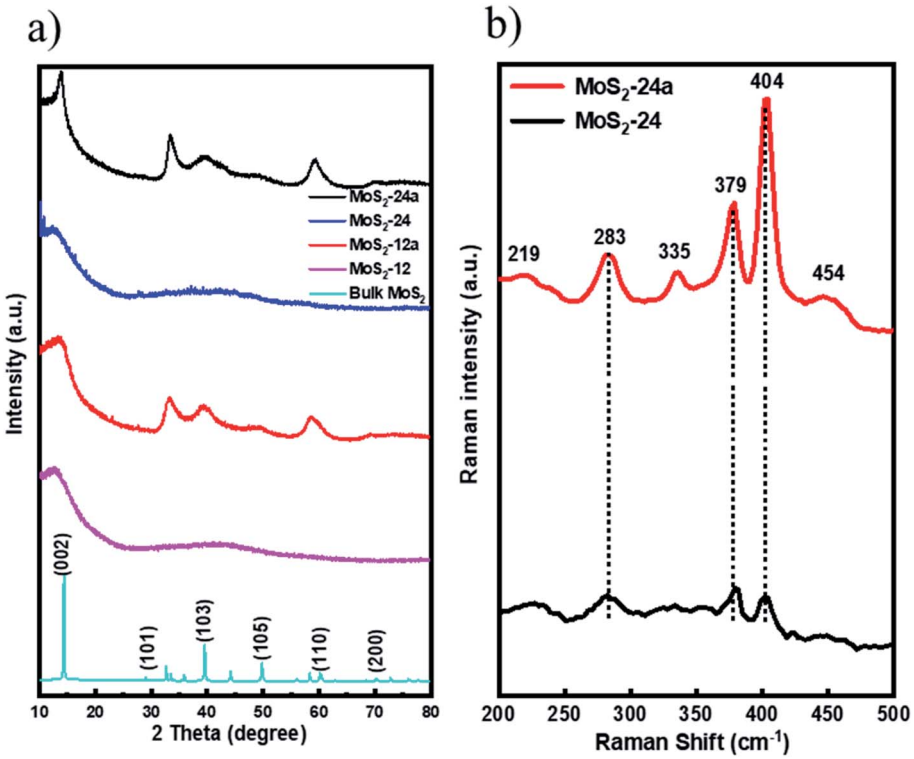

Fig. 1 (a) XRD patterns for MoS_2-12, MoS_2-12a, MoS_2-24, MoS_2-24a and bulk MoS_2 and (b) Raman spectra for MoS_2-24 and MoS_2-24a catalysts.

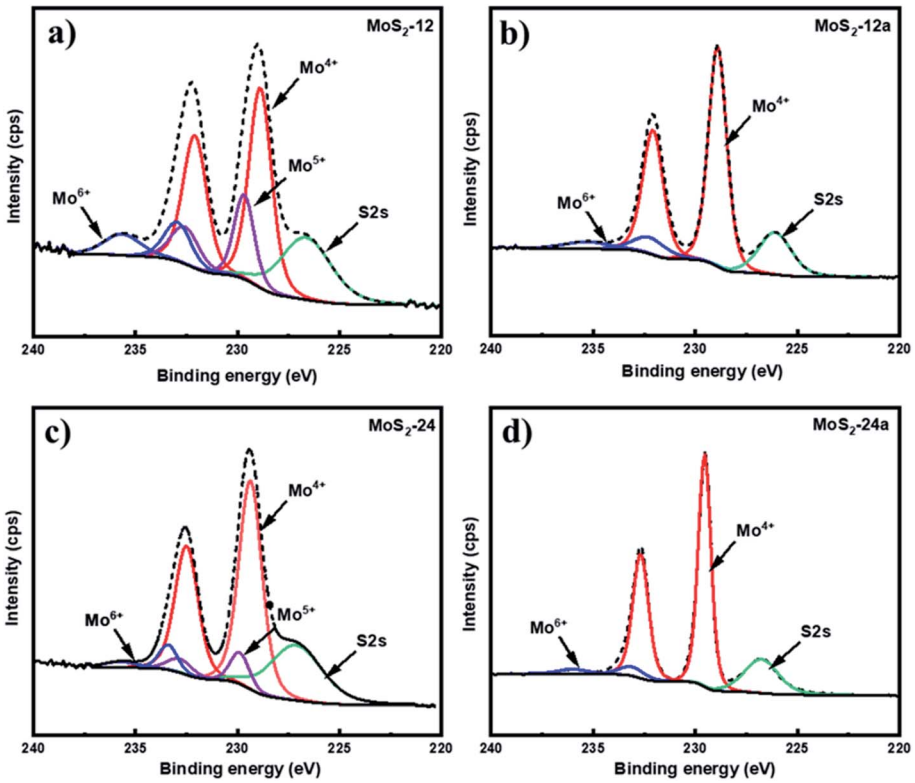

Fig. 2 XPS spectra of Mo 3d for (a) MoS_2-12, (b) MoS_2-12a, (c) MoS_2-24, and (d) MoS_2-24a.

Table 3 Mo 3d composition for MoS_2-12, MoS_2-12a, MoS_2-24, and MoS_2-24a

	Mo 3d composition (area %)		
Catalyst	Mo^{4+}	Mo^{5+}	Mo^{6+}
MoS_2-12	62.9	22.2	14.9
MoS_2-12a	88.6	—	11.4
MoS_2-24	82.9	11.3	5.8
MoS_2-24a	93.1	—	6.9

were not observed for both annealed catalysts. This result suggests that the MoO_xS_y phase may have been completely converted into MoS_3 and the annealing pretreatment can further facilitate the thermal decomposition of MoS_3 to MoS_2.

The morphologies of the unsupported catalysts in this study (Fig. 3) were examined by scanning electron microscopy (SEM). Spherical particle agglomerates can be observed in the SEM images which are due to the laminar growth of the MoS_2 during hydrothermal synthesis. The average particle diameter was measured based on the SEM images using ImageJ software and the distribution of the particle size is shown in the insets of Fig. 3. As can be seen in Fig. 3e and f, the MoS_2-24 catalyst, consists of a mixture of larger and smaller particles with an average particle diameter of 305 nm. A similar morphology can also be observed for MoS_2-12 (Fig. 3a and b). While for the MoS_2-24a catalyst, the SEM images revealed that the MoS_2 particles dispersed and distributed more uniformly with a smaller average particle diameter of 190 nm. A more defined morphology can also be observed in the annealed catalysts. The result suggested that the annealing treatment resulted in a reduction of particle diameter and a narrower size distribution of particles. To evaluate the influence of the pH adjustment on the morphology of MoS_2, a batch of unsupported MoS_2 was prepared following the same procedure, excluding the pH adjustment as described in the experimental section. The following batch was then examined by SEM and resulted in Fig. 4. A sharper and apparent flower-like morphology can be observed in the SEM image with a larger average particle diameter of 2 μm. Interestingly, this is almost the average particle size for the bulk MoS_2 sample (6 μm, max 40 μm). The results presented here are in line with the findings from Zhang *et al.*[43] The pH adjustment step in the catalyst synthesis was crucial to enhance the growth of MoS_2 micelles that eventually formed smaller crystallites in the MoS_2 catalysts. While the MoS_2 prepared without acid addition resulted in a larger particle size.

High-resolution transmission electron microscopy (HRTEM) was also performed to understand the effect of annealing on the structure of the unsupported catalyst, and the images are presented in Fig. 5. The usual thread-like fringes with an interplanar distance of 0.64 nm corresponding to the (0 0 2) basal planes of MoS_2 can be identified in all of the HRTEM images. One apparent difference that can be observed from the HRTEM images for the annealed catalysts was that the edges show a spiky feature that was not observed in the as-synthesized

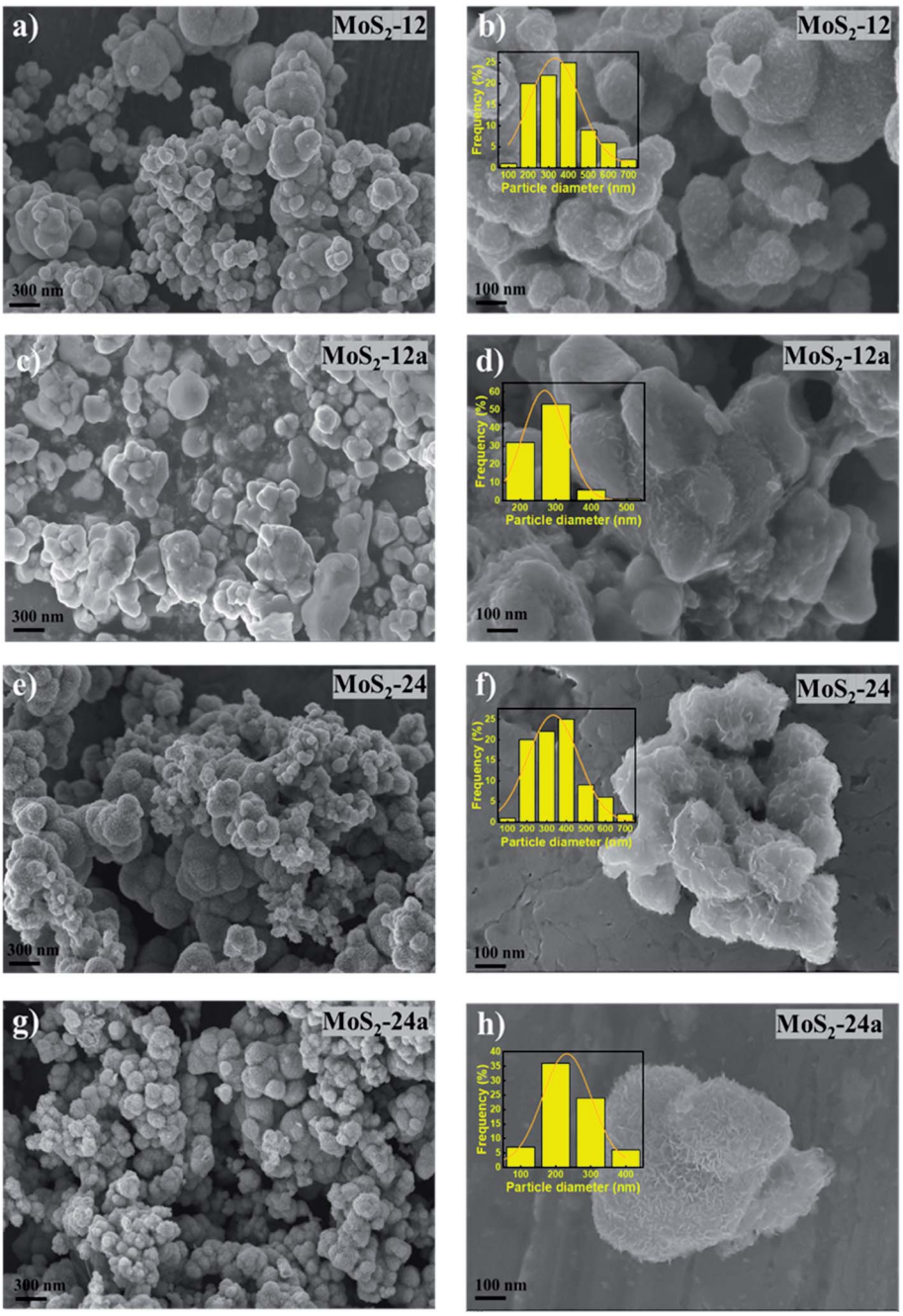

Fig. 3 SEM images of (a and b) MoS_2-12, (c and d) MoS_2-12a, (e and f) MoS_2-24, and (g and h) MoS_2-24a.

catalysts. This difference in the character of the edges of the as-synthesized and annealed catalysts is indicated by the arrows in Fig. 5. The red arrows indicated more rounded edges as can be observed for the as-synthesized catalysts. The yellow arrows indicated the sharp edges for the annealed catalysts. The changes in the structure near the edges of the catalyst after the annealing process could be due to the further enhancement in the growth of the smaller MoS_2 crystallites from the as-synthesized catalysts. This further demonstrates the importance of the annealing treatment that changes the structure of the catalysts. Consequently, the spiky edges of the annealed unsupported catalysts contribute to their higher specific surface area and exposure of more active sites for the HDO reaction. Owing to the interesting features of the as-synthesized and annealed catalysts, additional representative HRTEM micrographs (Fig. S3†) including 500–550 MoS_2 slabs were analyzed to study changes in the microstructure of the unsupported catalysts. The quantitative comparison of the average slab lengths, stacking layer number, MoS_2 dispersion, and the edge-to-corner of MoS_2 slabs are presented in Table 2. The distributions for the MoS_2 stacking numbers and slab length are shown in Fig. S4.† The average slab length for MoS_2 increases after the annealing

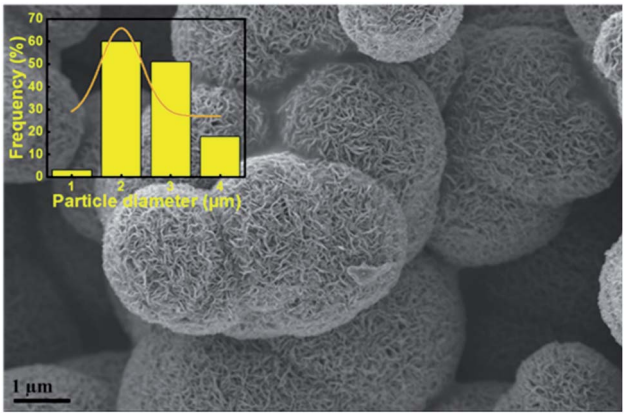

Fig. 4 SEM image for MoS_2 prepared without pH adjustment.

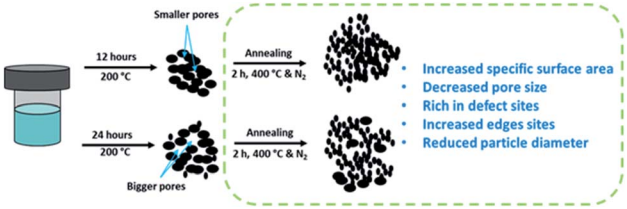

Scheme 1 Schematic illustration for the preparation of unsupported MoS_2 with annealing treatment.

treatment and the same trend was observed for both the 12 hours and 24 hours samples. The increase in average slab length also leads to a higher edge-to-corner ratio of MoS_2 slabs for both annealed samples. Both as-synthesized catalysts (MoS_2-12 and MoS_2-24) shown a 'defect-less' feature and a more curved multi-layered structure as indicated by the red arrows in the HRTEM images (Fig. S3†). On the other hand, the MoS_2 fringes in the annealed catalysts (MoS_2-12a and MoS_2-24a) are more randomly stacked and the sharp edges can be observed. These special features that can only be observed in the annealed catalysts confirm the greater presence of defect sites. The schematic illustration of the formation of unsupported MoS_2 and changes in properties due to the annealing treatment is shown in Scheme 1.

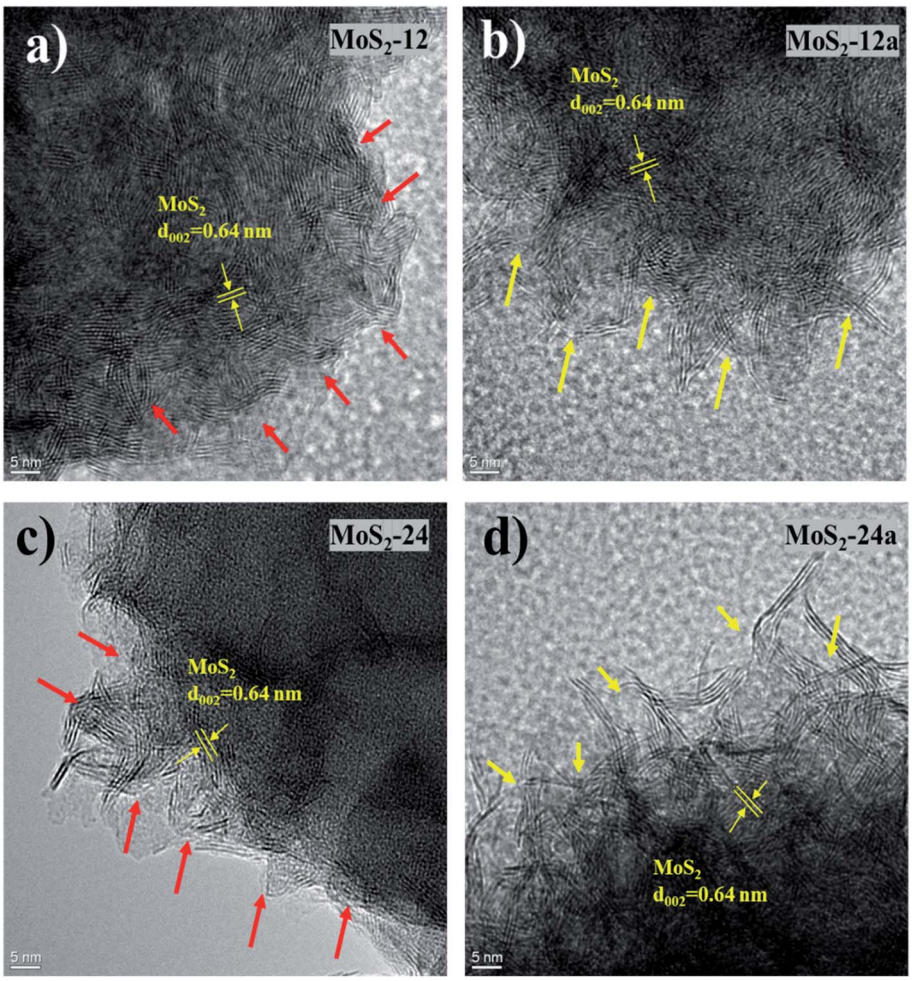

Fig. 5 HRTEM images of (a) MoS_2-12, (b) MoS_2-12a, (c) MoS_2-24, and (d) MoS_2-24a, with arrows indicating differences in characteristics of particle edges.

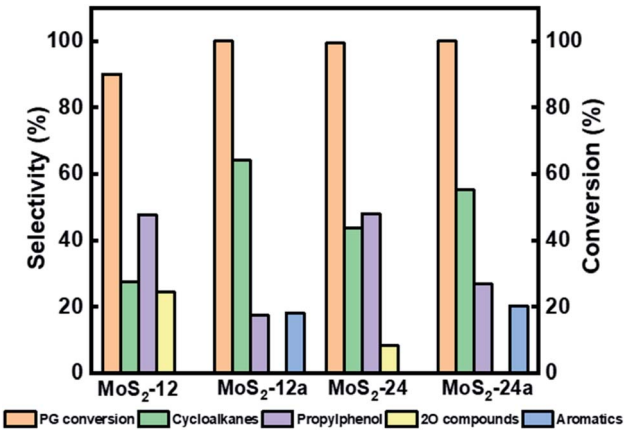

Fig. 6 Reaction product selectivity and conversion at 4 h for HDO of PG over MoS_2-12, MoS_2-12a, MoS_2-24, and MoS_2-24a at 50 bar total H_2 pressure, 300 °C, and 1000 rpm.

3.2 Catalytic performance test using 4-propylguaiacol and kraft lignin

3.2.1 Hydrodeoxygenation of 4-propylguaiacol (PG) over unsupported MoS_2 catalysts. The effects of catalyst synthesis time and the annealing pretreatment on the PG conversion and product selectivity were studied for HDO of 4-propylguaicol (PG) over unsupported MoS_2 at 50 bar total H_2 pressure, 300 °C and 1000 rpm. The reaction product selectivity and PG conversion after 4 h is illustrated in Fig. 6. Fig. 7 presents the time evolution of the conversion and product selectivity of the studied catalysts during a reaction period of 5 h. The deoxygenation route for PG occurred first *via* the removal of the methoxy group forming 4-propylphenol as the main initial intermediate. This observation indicates the initial preferential demethoxylation, followed by dehydroxylation since the methoxy bond connected to the phenyl ring is easier to break.[44] Then 4-propylphenol undergoes dehydroxylation producing 4-propylbenzene ('aromatics' in Fig. 6 and 7). The produced 4-propylbenzene was further hydrogenated forming 4-propylcyclohexene and 4-propylcyclohexane ('deoxygenated cycloalkanes' in Fig. 6 and 7). Reaction products that contain two oxygen atoms like 4-propylcatechol were also formed at the beginning of the reaction, but then their yield gradually decreased as the reaction proceeded. These products are referred to as '2O-compounds' in Fig. 6 and 7. A proposed reaction scheme for HDO of PG is shown in Scheme 2 based on the obtained results.

In Fig. 6, it can be seen that there was an improvement in the conversion of PG when the as-synthesized catalysts' synthesis

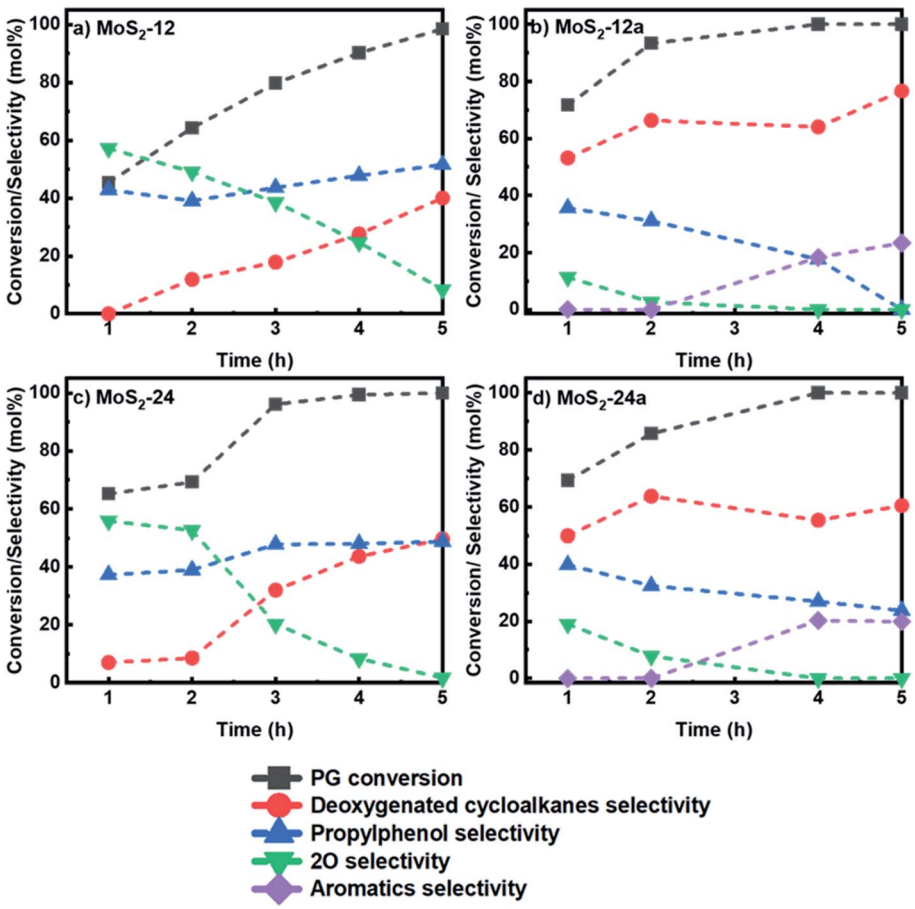

Fig. 7 Reaction product distribution for HDO of PG over (a) MoS_2-12 (b) MoS_2-12a (c) MoS_2-24 and (d) MoS_2-24a at 50 bar total H_2 pressure, 300 °C and 1000 rpm.

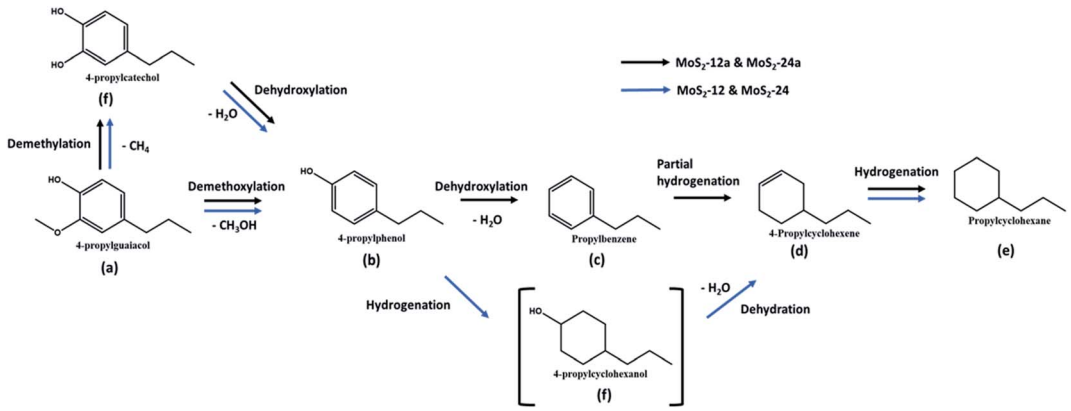

Scheme 2 Reaction scheme for HDO of PG over unsupported MoS_2 at 50 bar total H_2 pressure, 300 °C, and 1000 rpm.

time was increased from 12 h to 24 h. The PG conversion reached 90.1% using MoS_2-12, while almost complete conversion was achieved for MoS_2-24 after 4 h of reaction. There was also a difference in the selectivity for deoxygenated cycloalkanes like 4-propylcyclohexane and 4-propylcyclohexene where they were 27.5% and 43.4% for MoS_2-12 and MoS_2-24, respectively. On the other hand, the intermediate 4-propylphenol stayed in the range of between 47% and 48% selectivity after 4 h for both as-synthesized catalysts. In a previous study conducted by Wu *et al.*,[45] 34.7% selectivity for 4-propylphenol and 99.2% PG conversion were reported after 6 h of reaction at 300 °C showing a comparable result obtained with the as-synthesized catalyst in this study. The difference in results is likely due to the differences in the preparation methods, where they introduced silicomolybdic acid during the synthesis of their hydrophobic unsupported MoS_2 catalyst.[45] There was also a three times difference in the selectivity for 4-propylcatechol (2O-compound) with 24.7% for MoS_2-12 and decreasing to 8.3% for MoS_2-24, taking 4 h as a reference reaction time.

Both as-synthesized catalysts further underwent an annealing treatment at 400 °C for 2 h under nitrogen flow and were tested for HDO of PG. It can be noted from Fig. 7b and d that there was a change in product selectivity with a clear increase in cycloalkanes selectivity to 76.6% and 60.5% after 5 h for MoS_2-12a and MoS_2-24a, respectively as compared to the catalysts without the annealing treatment (40% and 49.6% for MoS_2-12 and MoS_2-24, respectively). The selectivity for 4-propylphenol also showed a downward trend for both the annealed catalysts. For the MoS_2-12a catalyst, 4-propylphenol, the major intermediate, was fully deoxygenated after 5 h while the selectivity of 4-propylcatechol gradually decreased and disappeared after 3 h. Whereas, for the HDO of PG over MoS_2-24a, the same downward trend for 4-propylphenol selectivity was observed with a final 23.8% remaining at the end of the reaction. Moreover, the selectivity for 4-propylcatechol (2O-compound) was low at the beginning of the reaction already at 1 h for both annealed catalysts (11.3% and 19.0% for MoS_2-12a and MoS_2-24a, respectively) as compared to the as-synthesized catalysts (57.2% and 55.8% for MoS_2-12 and MoS_2-24, respectively).

Interestingly, for both annealed catalysts, an aromatic compound (4-propylbenzene) could be identified after 2 h of reaction and its selectivity gradually increased reaching 23.4% and 19.8% for MoS_2-12a and MoS_2-24a, respectively after 5 h. The observed results showed that a 2 h annealing step improved the PG conversion and gave 19–24% selectivity for aromatic compounds with the same reaction parameters. The yield of fully deoxygenated products observed after 5 h decreased in the order of: MoS_2-12a (100%) > MoS_2-24a (80.4%) > MoS_2-24 (49.6%) > MoS_2-12 (40.0%). The absence of propylbenzene in the case of as-synthesized catalysts (MoS_2-12 and MoS_2-24) is mainly attributed to the higher amount of corner sites as indicated by the edge-to-corner sites ratio (Table 2) which is beneficial for hydrogenation reaction.[46] It was noteworthy that, one of the intermediates, 4-propylcyclohexanol was not detected in the reaction product. This suggests that 4-propylphenol was rapidly hydrogenated and deoxygenated to 4-propylcyclohexene and propylcyclohexane. The present data shows that the HDO activity and reaction routes are dependent largely on the MoS_2 morphology and a more favourable morphology is induced by a post thermal treatment of the as-synthesized catalysts as proposed in this work.

Additionally, for the as-synthesized catalysts, a longer synthesis time was preferred to achieve a better PG deoxygenation. While for the annealed catalysts, a shorter synthesis time was advantageous for PG deoxygenation. This could be reasoned by that the 12 h synthesis time is adequate to nucleate enough MoS_2 crystallites and the annealing treatment can facilitate the MoS_2 crystal growth with further rearrangement. Also, it is worth pointing out that MoS_2-12a achieved a full PG deoxygenation after 5 h even though the MoS_2-24a had a higher surface area while MoS_2-12a possessed the highest pore volume and the smallest pore size.

The difference in the catalytic performance of the annealed and as-synthesized unsupported MoS_2 catalysts depends largely on the MoS_2 morphology. For instance, the greater presence of defect sites as can be seen in the annealed catalysts in all the HRTEM images. These defect sites have been found to be important for creating more active sites, and further improving the HDO selectivity.[26] It should also be noted that these defect

sites contributed to the formation of additional edge active sites. It is noteworthy from the statistical analysis of the MoS_2 slabs (Table 2) for all catalysts that the annealing treatment increased the slab length of both MoS_2-12 and MoS_2-24. The longer MoS_2 slab length exhibited by the annealed catalysts correlates to the higher edge-to-corner ratio of the MoS_2 slabs. This also explained the higher HDO selectivity for both annealed catalysts which was attributed to the higher ratio of edge-to-corner of MoS_2 slabs. Thus, the annealing treatment proposed in this study was found to be able to create defect sites and further exposed MoS_2 edge sulfur vacancies for HDO activity enhancement.

To evaluate the performance of the unsupported MoS_2 prepared without the pH adjustment, both as-synthesized and annealed unsupported MoS_2 catalysts were employed for HDO of PG. The reaction product time evolution for both catalysts was measured, as shown in Fig. 8. A steady increase in PG conversion can be observed and a final PG conversion of 86.6% was obtained after 5 h for the as-synthesized MoS_2 prepared without acid addition. The selectivity for 4-propylphenol increased to 42.5% after 2 h and stabilized, reaching 40.8% at 5 h. A downward trend was observed for the selectivity for oxygenated intermediates (2O-compounds) giving a final selectivity of 19.5% (Fig. 8a). While for deoxygenated cycloalkanes product selectivity, a gradual increase in selectivity was observed achieving a final selectivity of 40%. The fresh as-synthesized MoS_2 (without acid) then underwent a similar annealing treatment as described previously and was applied for HDO of PG. Surprisingly, the annealing treatment, in this case, had a negative effect on the PG conversion, showing a final PG conversion of 74.2% after 5 h (Fig. 8b). Comparatively, there was a slight increase in the cycloalkanes selectivity, affording a final selectivity of 46.6% (Fig. 8b). While the selectivity for intermediate oxygenated compounds shows a decreasing trend with reaction time giving 36.6% selectivity for 4-propylphenol and 15.8% selectivity for 4-propylcatechol (2O-compounds) at the end of the reaction. From the clear difference in the product distribution for HDO of PG between the unsupported MoS_2 prepared in the presence and absence of acid addition, it can be concluded that creating an acidic environment while synthesizing unsupported MoS_2 is crucial to produce MoS_2 with smaller particle size. As for the MoS_2 particle size, the resulting surface has a direct effect on the HDO selectivity. This result is in line with the conclusion outlined by Zhang *et al.*,[43] which shows that higher HDS and hydrogenation activities can be achieved using MoS_2 prepared in low pH values. The smaller MoS_2 particles synthesized under an acidic environment possessed more active sites, leading to a higher HDO selectivity. It was also worth mentioning that the annealing treatment proposed in this study has a positive enhancement on the HDO activity while using MoS_2 prepared with pH adjustment. While for MoS_2 prepared without pH adjustment, it has an opposite effect, especially on the PG conversion and apparently in this case does not facilitate the growth of MoS_2 crystals.

Moreover, the effect of different pretreatment atmospheres on the PG product evolution and catalytic activity was investigated. The usual annealed MoS_2 catalysts in this study were all pretreated under continuous nitrogen flow. We performed an additional experiment where MoS_2-24 was annealed under air at 400 °C for 2 h and the PG conversion and products selectivity at 5 h are presented in Fig. S5.† PG was completely transformed after 5 h. Interestingly, a steady increase in the selectivity for 4-propylphenol can be observed, giving a final selectivity of 66.2%. High selectivity of 50% towards 4-propylcatechol (2O-compound) can be seen after 2 h which decreased abruptly to a final selectivity of 7%. The changes in the activity of the catalyst towards HDO could mainly be caused by changes in the nature and number of HDO active sites. These results also demonstrate the detrimental effect of an oxidative environment on the catalyst properties during annealing, which should result in producing more molybdenum oxysulfide species that are less favourable for HDO activity.[47]

To obtain a comparison in the HDO activity between the unsupported MoS_2 prepared in this work and commercially available bulk MoS_2, we performed the HDO of PG under the same reaction conditions over the bulk MoS_2, as shown in Fig. S6a.† Comparing the bulk MoS_2 and MoS_2-12a, the conversion of PG on bulk MoS_2 reached only 81.3% after 5 h,

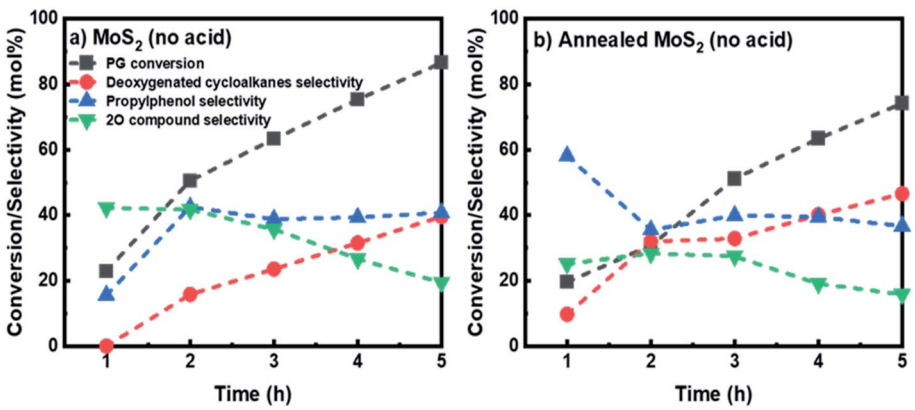

Fig. 8 Reaction product distribution for HDO of PG over (a) MoS_2 prepared without acid adjustment and (b) annealed MoS_2 without acid adjustment at 50 bar total H_2 pressure, 300 °C and 1000 rpm.

whereas for MoS_2-12a, PG was fully converted after 4 h. Selectivity for 4-propylphenol increased after 2 h and reached 44.8% after 5 h for bulk MoS_2. Selectivity for oxygenates like 4-propylcatechol (2O compound) was decreasing after 2 h and 26.9% remained at the end of the reaction. The poorer performance of the bulk MoS_2 could be reasoned by its 6 times lower specific surface area as compared to MoS_2-12a and its average particle size of 6 μm, which results in very limited active site accessibility. The current results show that the unsupported MoS_2 prepared in this work gives a superior PG conversion and higher deoxygenation activity as compared to the commercial bulk MoS_2.

The product distribution of unsupported MoS_2-12a and MoS_2 supported on Al_2O_3 (13.2 wt% Mo loading) catalyst was also compared. The experiments were performed with 500 mg and 66 mg of supported and unsupported catalysts, respectively. These different total masses of catalysts enabled a comparison of the catalysts based on an equal mass of the active component of Mo. The product evolution for the supported catalyst is shown in Fig. S6b.† The supported MoS_2/Al_2O_3 was prepared using a wetness impregnation method as described previously.[33] The use of a high surface area support during the synthesis of hydrotreatment catalysts ensures a high dispersion of the active phase that could provide more active sites for the HDO reaction to occur. A complete PG conversion was achieved after 2 h for the supported MoS_2/Al_2O_3 catalyst as compared to the 4 h needed for the unsupported MoS_2-12a. The selectivity for deoxygenated cycloalkanes also increased steadily from 38.8% to 70.2% during 5 h of reaction for the supported MoS_2. However, a two-fold higher aromatic selectivity (23.3%) could be obtained for MoS_2-12a at the end of the reaction. It was worth highlighting that the use of a high surface area alumina for supporting MoS_2 resulted in a faster PG conversion achieving full conversion in just 2 h. However, it should be noticed that PG was fully deoxygenated after 5 h in the case of the MoS_2-12a catalyst while 17.5% of 4-propylphenol selectivity can still be observed for the supported MoS_2 catalyst. These results show that a higher surface area is beneficial in improving the transformation of PG to various compounds but not the HDO activity. This is consistent with the conclusion made by Wang *et al.*,[27] stating that a higher specific surface area may not be the major factor in giving high HDO activity. Also, the active site density per mass active phase (MoS_2) with the supported catalyst may be higher since it gives a higher PG conversion, however, the nature of these sites is undoubtedly different since the unsupported catalyst gave a higher degree of deoxygenation.

3.2.2 Hydrotreatment of kraft lignin over an unsupported MoS_2 and bulk MoS_2. To extend the scope of the application of the annealed unsupported MoS_2 to a more complex and realistic bio-feedstock, kraft lignin was selected, which contains an array of oxygenates (hydroxyl, methoxy and various oxygenate linkages). Both MoS_2-12a and bulk MoS_2 were employed in the hydrotreatment of kraft lignin at 340 °C and 40 bar initial H_2 pressure. The focus was on the analysis of the upgraded lignin oil fraction and quantifying its main groups of product compounds. A complete kraft lignin conversion could be observed after 5 h of hydrotreatment for both catalysts, forming bio-oils and char. A 43% char yield was obtained for commercial bulk MoS_2 while it dropped to 27% for MoS_2-12a. Fig. 9 presents a comparison between the selectivity of cycloalkanes, aromatics, and phenolic compounds obtained for both unsupported catalysts. The results indicate a notable difference between the chemical compositions of the upgraded lignin oil fractions. Due to the complexity of the lignin feed, a wide range of monomer and dimer products were expected from the lignin depolymerization due to hydrotreatment. Table S2† listed all the compounds in the lignin oil fraction that were identified and detected by the GC-MS according to their retention times with their individual selectivities (in terms of relative FID peak area %). The GC spectra for both catalysts are shown in Fig. S7.† The noticeable difference between both catalysts was that the major compounds in the lignin oil fraction for MoS_2-12a were both cycloalkanes (*e.g.* methylcyclopentane, cyclohexane, methylcyclohexane, ethylcyclopentane, ethylcyclohexane, and propylcyclohexane) and aromatic compounds (*e.g.* toluene, 1,3-dimethylbenzene, and propylbenzene). However, for the bulk MoS_2 catalysts, oxygenates like guaiacol, creosol, 4-ethyl-2-methoxyphenol and propylguaiacol were the major compounds that remained in the lignin product mixture. All of the identified compounds in the GC spectrum were grouped and classified into cycloalkanes, aromatics, and phenolic compound groups as presented in Fig. 9. The reaction products were also subjected to 2D GC × GC analysis and the results as shown in Fig. 10 giving a qualitative illustration of the different product distributions. It is clearly visible from Fig. 10 that there is a difference in product distribution between bulk MoS_2 and MoS_2-12a. The major products that can be observed in the GC × GC chromatogram for bulk MoS_2 (Fig. 10a) represented mainly phenolics components like guaiacol-derived components and alkylphenols. On the other hand, the highlighted blobs in the GC × GC chromatogram for MoS_2-12a (Fig. 10b) are associated with deoxygenated compounds like naphthenes and aromatics with traces of polyaromatics. The blob intensities for oxygenates

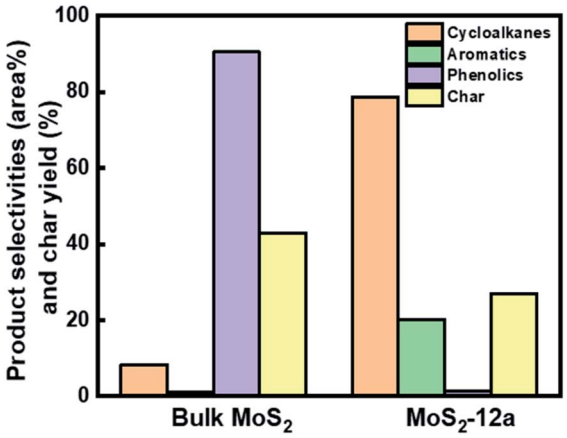

Fig. 9 GCMS analysis for the comparison of product selectivities and char yield between bulk MoS_2 and MoS_2-12a for hydrotreatment of kraft lignin. Reaction conditions: 3 : 1 lignin to catalyst mass ratio, 340 °C, 40 bar initial H_2 pressure, 5 h, and 1000 rpm.

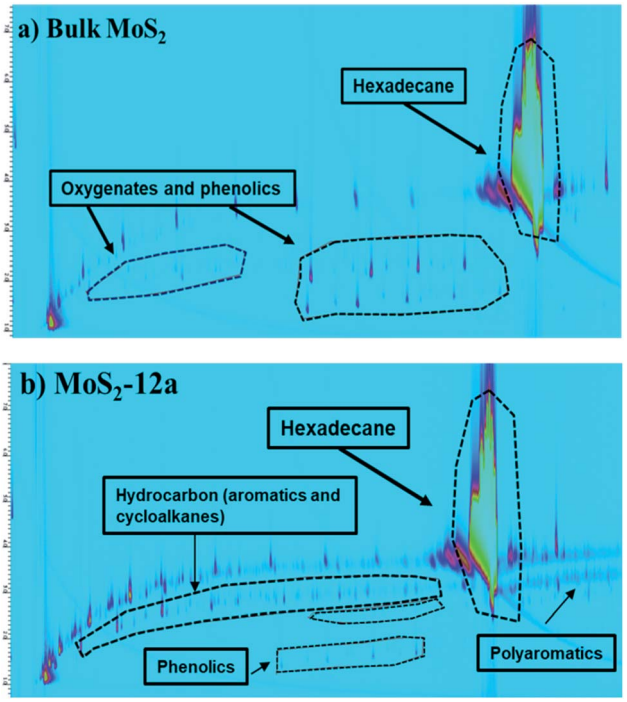

Fig. 10 Chromatograms (2D GC × GC-MS-FID) of the reaction liquid products obtained in the hydrotreatment of kraft lignin over (a) Bulk MoS_2 and (b) MoS_2-12a.

are clearly reduced as can be seen in the chromatograms for MoS_2-12a (Fig. 10b). A total selectivity of 90.5% for phenolics compounds and only 8.3% of cycloalkanes were observed using the bulk MoS_2. In contrast, 78.6% of cycloalkanes and 20.1% of aromatic selectivity were achieved in the case of MoS_2-12a.

The higher deoxygenation achieved in kraft lignin hydrotreatment for the annealed unsupported MoS_2-12a as compared to the bulk MoS_2 is consistent with the results for the model reaction, HDO of PG. Also, the formation of carbonaceous solid products (char) from the re-polymerization or condensation of lignin fragments is less in the case of the synthesized unsupported MoS_2. This indicates that a catalyst with high activity and accessibility of sites for deoxygenation and hydrogenation reactions is important to prevent these char formation reactions.

4. Conclusions

In summary, a facile hydrothermal synthesis method has been successfully employed to prepare unsupported MoS_2 catalysts and the work also revealed the significance of a post-thermal annealing treatment to the as-synthesized catalysts for enhancing HDO performance. Increasing the synthesis time from 12 h to 24 h has an overall positive effect on the PG conversion and deoxygenated cycloalkanes selectivity. For instance, a complete PG conversion was achieved using MoS_2-24, while 90.1% PG conversion was obtained for MoS_2-12 after 4 h. There was also a 1.6-fold higher deoxygenated cycloalkanes selectivity for MoS_2-24 as compared to MoS_2-12 after 4 h of reaction. An annealing treatment of the as-synthesized catalysts performed at 400 °C for 2 h under nitrogen atmosphere was found to have a remarkable effect on the HDO activity. The present results in this work indicated that the annealing treatment was found to be effective in the creation of a greater abundance of defect sites that further enhance HDO activity. An increase in deoxygenated cycloalkane selectivity was observed for both annealed samples, with 76.6% for MoS_2-12a and 60.5% for MoS_2-24a after 5 h. Moreover, an aromatic compound like 4-propylbenzene could be detected for both annealed samples after 2 h which was not the case for the as-synthesized catalysts. The MoS_2 morphology change caused by the annealing for both as synthesized catalysts also contributed to differences in HDO activity and reaction routes. The fully deoxygenated product yields after 5 h was ranked in the following order: MoS_2-12a (100%) > MoS_2-24a (80.4%) > MoS_2-24 (49.6%) > MoS_2-12 (40.0%). It was found that the longer synthesis time was advantageous to achieve a higher PG deoxygenation for as-synthesized catalysts, however for the annealed samples, a shorter synthesis time was better. It can be hypothesized that 12 h synthesis time is sufficient to nucleate enough MoS_2 crystals that undergo crystallite growth and rearrangement during the annealing treatment for a high yield of optimal crystal size and morphology for HDO activity. Also, the acidic environment during the synthesis was important to promote the growth of MoS_2 crystals which has a direct effect on the HDO activity. The effect of annealing on the samples prepared without pH adjustment was studied and it was shown to have an adverse effect on the PG conversion and therefore did not facilitate the further growth of the MoS_2 crystallites.

There was an increase in crystallinity of MoS_2 after the annealing treatment based on XRD analysis. These changes were consistent with observations of particle size and MoS_2 structure according to SEM and TEM analysis. The MoS_2 particles had a more uniform and reduced average particle size after the annealing treatment. The absence of the molybdenum oxysulfide species in the annealed catalysts was consistent with higher MoS_2 yield and improved activity for HDO of PG. The clear difference in product distribution and selectivity for MoS_2 annealed under nitrogen and air atmosphere suggested that an inert environment during annealing was vital to avoid oxidation during the annealing process. We further compared the HDO activity between the unsupported MoS_2 with alumina-supported MoS_2, using the same Mo content in both experiments, and concluded the differences in the nature of the active sites of the catalysts may explain their different final degrees of deoxygenation.

Additionally, the application of the annealed MoS_2 was further demonstrated in the hydrotreatment of kraft lignin. The higher deoxygenation activity of the annealed unsupported MoS_2 was found to be vital for achieving a lower char yield from the lignin. The high selectivity for deoxygenated products in the liquid products revealed the feasibility of utilizing unsupported catalytic materials for the upgrading of renewable bio-feedstocks.

Conflicts of interest

There are no conflicts to declare.

Acknowledgements

This research is a collaboration work between Competence Centre for Catalysis (KCK) at Chalmers, Preem AB, and RISE Energy Technology Center (ETC). The authors would like to acknowledge the Swedish Energy Agency (2017-010890) and Preem AB for financial support. This work was also performed in part at the Chalmers Material Analysis Laboratory, CMAL for SEM, TEM, XPS, Raman, and XRD analysis.

References

1 IEA, *World Energy Outlook 2019*, 2019, IEA, Paris, https://www.iea.org/reports/world-energy-outlook-2019.
2 L. Fan, Y. Zhang, S. Liu, N. Zhou, P. Chen, Y. Cheng, M. Addy, Q. Lu, M. M. Omar, Y. Liu, Y. Wang, L. Dai, E. Anderson, P. Peng, H. Lei and R. Ruan, *Bioresour. Technol.*, 2017, **241**, 1118–1126.
3 F. S. Chakar and A. J. Ragauskas, *Ind. Crops Prod.*, 2004, **20**, 131–141.
4 G. W. Huber, S. Iborra and A. Corma, *Chem. Rev.*, 2006, **106**, 4044–4098.
5 P. Sudarsanam, R. Zhong, S. Van Den Bosch, S. M. Coman, V. I. Parvulescu and B. F. Sels, *Chem. Soc. Rev.*, 2018, **47**, 8349–8402.
6 M. Saidi, F. Samimi, D. Karimipourfard, T. Nimmanwudipong, B. C. Gates and M. R. Rahimpour, *Energy Environ. Sci.*, 2014, **7**, 103–129.
7 P. Mäki-Arvela and D. Murzin, *Catalysts*, 2017, **7**(9), 265.
8 E. Furimsky, *Appl. Catal., A*, 2000, **199**, 147–190.
9 W. O. S. Doherty, P. Mousavioun and C. M. Fellows, *Ind. Crops Prod.*, 2011, **33**, 259–276.
10 D. Laurenti, B. Phung-Ngoc, C. Roukoss, E. Devers, K. Marchand, L. Massin, L. Lemaitre, C. Legens, A. A. Quoineaud and M. Vrinat, *J. Catal.*, 2013, **297**, 165–175.
11 P. E. Ruiz, B. G. Frederick, W. J. De Sisto, R. N. Austin, L. R. Radovic, K. Leiva, R. García, N. Escalona and M. C. Wheeler, *Catal. Commun.*, 2012, **27**, 44–48.
12 S. Mukundan, M. Konarova, L. Atanda, Q. Ma and J. Beltramini, *Catal. Sci. Technol.*, 2015, 4422–4432.
13 G. M. K. Abotsi and A. W. Scaroni, *Fuel Process. Technol.*, 1989, **22**, 107–133.
14 S. Mukundan, L. Atanda and J. Beltramini, *Sustainable Energy Fuels*, 2019, **3**, 1317–1328.
15 G. Zhu, W. Wang, K. Wu, S. Tan, L. Tan and Y. Yang, *Ind. Eng. Chem. Res.*, 2016, **55**, 12173–12182.
16 S. Eijsbouts, S. W. Mayo and K. Fujita, *Appl. Catal., A*, 2007, **322**, 58–66.
17 F. L. Plantenga, R. Cerfontain, S. Eijsbouts, F. Van Houtert, G. H. Anderson, S. Miseo, S. Soled, K. Riley, K. Fujita and Y. Inoue, *Stud. Surf. Sci. Catal.*, 2003, **145**, 846–849.
18 G. Bellussi, G. Rispoli, A. Landoni, R. Millini, D. Molinari, E. Montanari, D. Moscotti and P. Pollesel, *J. Catal.*, 2013, **308**, 189–200.
19 N. Bergvall, L. Sandström, F. Weiland and O. Öhrman, *Energy Fuels*, 2020, **34**, 8452–8465.
20 C. Mattsson, S. I. Andersson, T. Belkheiri, L. E. Åmand, L. Olausson, L. Vamling and H. Theliander, *Biomass Bioenergy*, 2016, **95**, 364–377.
21 F. L. P. Resende, S. A. Fraley, M. J. Berger and P. E. Savage, *Energy Fuels*, 2008, **22**, 1328–1334.
22 A. Demirbaş, *Energy Convers. Manage.*, 2000, **41**, 1601–1607.
23 A. N. Varakin, A. V. Mozhaev, A. A. Pimerzin and P. A. Nikulshin, *Catal. Today*, 2019, 1.
24 B. Yoosuk, D. Tumnantong and P. Prasassarakich, *Chem. Eng. Sci.*, 2012, **79**, 1–7.
25 M. Grilc, G. Veryasov, B. Likozar, A. Jesih and J. Levec, *Appl. Catal., B*, 2015, **163**, 467–477.
26 C. Zhang, K. Liu, Y. Zhang, L. Mu, Z. Zhang and J. Huang, *Appl. Catal., A*, 2021, **621**, 118175.
27 W. Wang, K. Zhang, L. Li, K. Wu, P. Liu and Y. Yang, *Ind. Eng. Chem. Res.*, 2014, **53**, 19001–19009.
28 K. Wu, W. Wang, H. Guo, Y. Yang, Y. Huang, W. Li and C. Li, *ACS Energy Lett.*, 2020, **5**, 1330–1336.
29 W. Wang, L. Li, K. Wu, G. Zhu, S. Tan, W. Li and Y. Yang, *RSC Adv.*, 2015, **5**, 61799–61807.
30 J. Cao, A. Li, Y. Zhang, L. Mu, X. Huang, Y. Li, T. Yang, C. Zhang and C. Zhou, *Mol. Catal.*, 2021, **505**, 1–9.
31 H. Wang, K. Rogers, H. Zhang, G. Li, J. Pu, H. Zheng, H. Lin, Y. Zheng and S. Ng, *Mol. Catal.*, 2017, **443**, 228–240.
32 W. Wang, K. Zhang, Z. Qiao, L. Li, P. Liu and Y. Yang, *Catal. Commun.*, 2014, **56**, 17–22.
33 Y. W. Cheah, M. A. Salam, P. Arora, O. Öhrman, D. Creaser and L. Olsson, *Sustainable Energy Fuels*, 2021, **5**, 2097–2113.
34 P. Arora, H. Ojagh, J. Woo, E. Lind Grennfelt, L. Olsson and D. Creaser, *Appl. Catal., B*, 2018, **227**, 240–251.
35 M. A. Salam, P. Arora, H. Ojagh, Y. W. Cheah, L. Olsson and D. Creaser, *Sustainable Energy Fuels*, 2020, **4**, 149–163.
36 D. Ferdous, A. K. Dalai, J. Adjaye and L. Kotlyar, *Appl. Catal., A*, 2005, **294**, 80–91.
37 M. Kruk and M. Jaroniec, *Chem. Mater.*, 2001, **31**(10), 3169–3183.
38 H. Lin, X. Chen, H. Li, M. Yang and Y. Qi, *Mater. Lett.*, 2010, **64**, 1748–1750.
39 A. Jagminas, G. Niaura, R. Žalneravičius, R. Trusovas, G. Račiukaitis and V. Jasulaitiene, *Sci. Rep.*, 2016, **6**, 2–10.
40 G. M. Bremmer, L. van Haandel, E. J. M. Hensen, J. W. M. Frenken and P. J. Kooyman, *Appl. Catal., B*, 2019, **243**, 145–150.
41 L. Benoist, D. Gonbeau, G. Pfister-Guillouzo, E. Schmidt, G. Meunier and A. Levasseur, *Solid State Ionics*, 1995, **76**, 81–89.
42 F. Solymosi, J. Cserényi, A. Szöke, T. Bánsági and A. Oszkó, *J. Catal.*, 1997, **165**, 150–161.
43 C. Zhang, P. Li, X. Liu, T. Liu, Z. Jiang and C. Li, *Appl. Catal., A*, 2018, **556**, 20–28.
44 L. Bomont, M. Alda-Onggar, V. Fedorov, A. Aho, J. Peltonen, K. Eränen, M. Peurla, N. Kumar, J. Wärnå, V. Russo, P. Mäki-Arvela, H. Grénman, M. Lindblad and D. Y. Murzin, *Eur. J. Inorg. Chem.*, 2018, (24), 2841–2854.
45 K. Wu, Y. Liu, W. Wang, Y. Huang, W. Li, Q. Shi and Y. Yang, *Mol. Catal.*, 2019, **477**, 110537.

46 E. J. M. Hensen, P. J. Kooyman, Y. Van der Meer, A. M. Van der Kraan, V. H. J. De Beer, J. A. R. Van Veen, R. A. Van Santen, P. J. Kooyman, Y. Van der Meer and A. M. Van der Kraan, *J. Catal.*, 2001, **199**, 224–235.
47 M. Sugioka and F. Kimura, *J. Jpn. Pet. Inst.*, 1985, **28**, 306–311.
48 T. Burimsitthigul, B. Yoosuk, C. Ngamcharussrivichai and P. Prasassarakich, *Renewable Energy*, 2021, **163**, 1648–1659.
49 B. Yoosuk, P. Sanggam, S. Wiengket and P. Prasassarakich, *Renewable Energy*, 2019, **139**, 1391–1399.
50 B. Yoosuk, D. Tumnantong and P. Prasassarakich, *Chem. Eng. Sci.*, 2012, **79**, 1–7.

